2022-01-0503 Published 29 Mar 2022

Applying Physics-Informed Enhanced Super-Resolution Generative Adversarial Networks to Large-Eddy Simulations of ECN Spray C

Mathis Bode Jülich Supercomputing Centre, Forschungszentrum Jülich GmbH; RWTH Aachen University

Citation: Bode, M., "Applying Physics-Informed Enhanced Super-Resolution Generative Adversarial Networks to Large-Eddy Simulations of ECN Spray C," *SAE Int. J. Advances & Curr. Prac. in Mobility* 4(6):2211-2219, 2022, doi:10.4271/2022-01-0503.

This article was presented at the WCX World Congress Experience, April 5-7, 2022.

Received: 06 Nov 2021 Revised: 09 Jan 2022 Accepted: 17 Jan 2022

Abstract

Large-eddy simulation (LES) is an important tool to understand and analyze sprays, such as those found in engines. Subfilter models are crucial for the accuracy of spray-LES, thereby signifying the importance of their development for predictive spray-LES. Recently, new subfilter models based on physics-informed generative adversarial networks (GANs) were developed, known as physics-informed enhanced super-resolution GANs (PIESRGANs). These models were successfully applied to the Spray A case defined by the Engine Combustion Network (ECN). This work presents technical details of this novel method, which are relevant for the modeling of spray combustion, and applies PIESRGANs to the ECN Spray C case. The results are validated against experimental data, and computational challenges and advantages are particularly emphasized compared to classical simulation approaches.

Introduction

In order to accurately calculate complex flows with multi-physical phenomena using direct numerical simulation (DNS), all relevant time and length scales must be resolved. This is not possible for many cases within an acceptable runtime regardless of the extensive computing capacities available today. Consequently, large-eddy simulation (LES) has established itself as a fair approach for turbulent, reactive flows, since it significantly reduces the required computational capacity. In this case, scales of various magnitudes are separated from each other by utilizing a filter operation. During the simulation, equations for the coarser scales are solved, and the influence of the finer scales is modeled without fully resolving them. Therefore, a major task in the context of predictive simulations is the development of suitable models that reliably represent the effect of the finer scales on the coarser scales.

Since more and larger amounts of data are being generated and data analysis tools are significantly improved by recent developments focusing on artificial intelligence, data-driven model building is becoming increasingly popular [1, 2]. For example, data generated using DNS describing turbulent mixing can be used to develop a corresponding LES mixing model. To have maximum flexibility, Deep Learning (DL) networks can be employed for this purpose. These networks can represent very complex, non-linear objective functions and consider a wide data input space, as has already been demonstrated in many recent use cases from different scientific fields [3-6].

These data-driven approaches have also been applied to fluid dynamics problems [7-10], including works on subfilter modeling for LES [11-13] based on DNS data. Recently, the idea of physics- informed networks [14] has emerged, where architecture or loss functions are designed to support known properties of underlying physical problems.

Neural networks have also been applied successfully to reactive flows. Some examples are the adaptive reduction scheme for modeling reactive flows by Banerjee et al. [15], artificial neural network (ANN)-based storage of flamelet solutions [16, 17], and direct mapping of LES resolved scales to filtered-flame generated manifolds using customized convolutional neural networks (CNNs) as shown by Seltz et al. [18]. Additionally, regularized deconvolution methods, such as those published by Wang and Ihme [19], are closely related ideas to subfilter modeling approach in this work.

PIESRGANs (Physics-Informed Enhanced Super-Resolution Generative Adversarial Networks) have been recently developed and show high predictive accuracy for LES modeling in turbulent reactive flows [13, 20]. Similar to all GANs (Generative Adversarial Networks) [21], PIESRGAN uses two DL networks that play a zero-sum game during model building to finish with a very accurate generator network for an LES. For this, it is particularly important that the model building process, also known as

training, is performed effectively. Although the models based on PIESRGANs shown thus far are very promising, many questions remain unanswered and require further research.

LES models are also critical for the prediction of engine-type sprays. Fully resolving all relevant scales is usually neither possible nor productive during an engine development or optimization process. Davidovic et al. [22] showed that the early mixing for the Engine Combustion Network (ECN) [23] Spray A case is not trivial to model accurately with classical LES models. Bode et al. [20] investigated this effect even further and demonstrated that PIESRGAN-based LES models have significant advantages for the mixture prediction on coarse meshes. This work discusses the advantages and shortcomings of PIESRGAN in terms of computational performance in more detail, as well as describes its application to the ECN Spray C case. As Spray C is more complex than Spray A, featuring cavitation and a shorter lift-off length (LOL), this study will depict that PIESRGAN also works well in this case. Additionally, it will be interesting to observe how the simplified setup without nozzle flow coupling operates, as it is known that the Spray C plume is tilted, presumably due to low pressure regions at the orifice originating from cavitation [23].

This paper continues with a description of PIESRGANs, including combustion. Afterwards, details about the used turbulence data and implementation are briefly stated. The discussion part addresses the generality and universality properties of PIESRGAN, its accuracy with respect to mixture prediction, and its computational performance during training and on runtime. Subsequently, results of the ECN Spray C case are shown. The paper ends with conclusions.

Modeling

In this chapter, the turbulence and combustion modeling approaches are described.

Turbulence

The effects in turbulent flows can be described by the Navier-Stokes equations and are coupled across all scales. This implies that all scales must be resolved simultaneously in simulations to obtain accurate solutions. For non-reactive single-phase turbulent flows without further multi-physical effects, the scale separation between coarse and fine scales is definable by the Reynolds number, i.e., the larger the Reynolds number, the larger the scale separation. Here, the smallest scale is represented by the Kolmogorov length and time. For flows with multi-physical effects, such as combustion, the scale separation can increase even more since the scalar mixing can take place on even finer scales, or a flame thinner than the Kolmogorov length can be established.

To reduce the enormous computational cost of very fine grids necessary due to the scale separation, LES separates the individual scales by a filter operation Ξ. During simulation, the filtered Navier-Stokes equations are solved on a grid, which does not resolve the fine scales; consequently, the equations contain unclosed terms that cannot be determined without knowledge of the fine scales, and thus must be modeled. This is cost effective, but the accuracy of the results is highly dependent on the subfilter models employed for the unclosed terms.

PIESRGANs provide a novel approach to develop subfilter models for LES. The modeling idea is to estimate an inverse filtering operation Ξ^{-1} that adds the information that was filtered out back to filtered data ("F"). The resulting reconstructed data ("R") can then be used to exactly close the unclosed terms in the filtered equations, assuming an exact approximation. Indeed, this addition of information is non-trivial and not possible with a simple "algebraic" model. Thus, in the context of PIESRGAN-LES models, the hypothesis is that the inverse filtering operation can be approximated sufficiently accurately with a suitable DL-model and appropriate training data. It is essentially based on the physical notion that turbulence is statistically universal at the finest scales [24, 25], only depending on the viscosity and the mean scalar dissipation rate of the turbulent kinetic energy, which makes it possible to train the model on generic data and then apply it to different technical applications. The individual modeling steps are summarized in Table 1.

The results of the PIESRGAN model depend significantly on four factors: the network architecture, the implied physical constraints, the base training data ("H"), and the additional training data ("S"). The network architecture of PIESRGAN is based on ESRGANs (Enhanced Super-Resolution GANs) [3], which were originally designed to increase the resolution in two-dimensional (2-D) everyday images. Like any GAN, PIESRGAN has a generator network (Figure 1) and a discriminator network (Figure 2). Both significantly use Conv3D (3D Convolutional Layer) components with activation functions. In the generator network, these are combined to form DBs (Dense Blocks), RDBs (Residual Dense Blocks), and finally an RRDB (Residual in Residual Dense Block). The discriminator network uses BN (Batch Normalization) components, Dense components ("Fully Connected Layer"), and a dropout for regularization in addition to the Conv3D components. Both networks are coupled via the "adversarial" loss term in the loss functions, where the loss function of a network is the objective function that is minimized to optimize the parameters of the networks over all training data.

In general, the loss functions of both networks can be expressed as

$$L = \beta_1 L_{\text{adversarial}} + \beta_2 L_{\text{pixel}} + \beta_3 L_{\text{gradient}} + \beta_4 L_{\text{physics}} \quad (1)$$

with four loss terms, where $\beta_1 \ldots \beta_4$ are the weight factors of the individual loss terms and sum to one. Here,

TABLE 1 PIESRGAN modeling steps using the example of the time evolution from n to n+1 of a quantity ϕ with unclosed terms ψ in the associated filtered equation.

Step	Action	Description
1	Reconstruction	Reconstruct ϕ_R^n from ϕ_F^n using PIESRGAN
2	Evaluation	Use ϕ_R^n and a filter operation to compute ψ_F^n
3	Advancement	Advance ϕ_F^{n+1} with the filtered equations, ϕ_F^n and ψ_F^n

FIGURE 1 Schematic representation of the PIESRGAN generator network: Conv3D - 3D Convolutional Layer, LeakyReLU - Activation Function, DB - Dense Block, RDB - Residual Dense Block, RRDB - Residual in Residual Dense Block, β_{RSF} - Residual Scaling Factor.

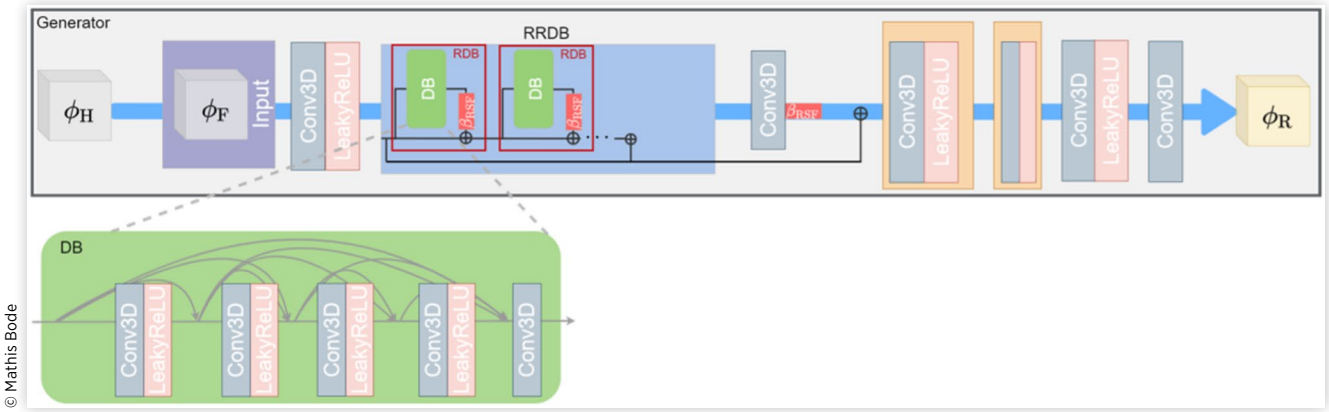

FIGURE 2 Schematic representation of the PIESRGAN discriminator network: Conv3D - 3D Convolutional Layer, LeakyReLU - Activation Function, BN - Batch Normalization, Dense - Fully Connected Layer, Dropout - Regularization Component, $\beta_{dropout}$ - Dropout Factor.

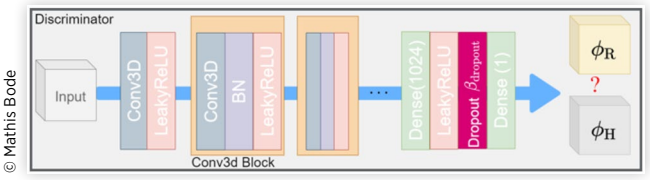

$L_{adversarial}$ stands for the adversarial loss typical of GANs, L_{pixel} is the integral point-wise defined loss based on the target data field, $L_{gradient}$ depicts an integral point-wise defined loss based on the gradient of the target data field, and $L_{physics}$ is the set of certain problem-specific losses that are physically motivated. For example, PIESRGAN may use a loss to ensure mass conservation in the reconstructed data field. This physically motivated modification of the loss functions is particularly significant in the context of subfilter modeling for LES relative to other traditional computer science applications to minimize certain errors as much as possible, since they would otherwise lead to numerically unstable simulations.

The base training data is usually high-resolution data that can be determined using DNS or experimental methods. It is filtered to obtain pairs of data required in order to train the networks. The networks are provided with the filtered data and continuously optimized to reconstruct the resolved data with respect to the loss functions as the amount of data increases. For the evaluations of the loss functions, the corresponding high-resolution data, which serve as the "exact" solution, must generally be known. DNS data of homogeneous isotropic turbulence in a box has proven to be good base training data.

In an additional training step, other data can be used to further increase the accuracy of PIESRGANs. Here, it is also possible to optimize only the generator network and continue without a further update of the discriminator network. In this particular training step, the adversarial loss is then often of special importance, as will be discussed in the discussion chapter.

Further details on PIESRGANs, such as the normalization of the individual variables, determination of the factors and effects of individual network components, are described in the studies conducted by Bode et al. [13, 20].

Combustion

Chemistry is modeled by means of a multiple representative interactive flamelets (MRIF) approach. The general approach is summarized in Figure 3, and further details can be found in previous publications [22, 26]. In simple terms, the flow solver and the chemistry solver are only loosely coupled by the scalar dissipation rate χ in flamelet approaches, and an equation for the mixture fraction Z (and usually its variance) is solved as part of the LES, which allows to solve the chemistry in 1-D mixture fraction space instead of 3-D physical space. One consecutive challenge is to accurately remap the solutions computed in mixture fraction space on the physical space. Usually, this is done by constructing a presumed β-PDF (probability density function) depending on the local filtered mixture fraction and mixture fraction variance. However, this functional form is an obvious approximation. Thus, in this work, the remapping is done based on the reconstructed mixture fraction field combined with a filter operation, reducing the required level of a priori knowledge significantly.

This work only aims to demonstrate the applicability of PIESRGAN for advanced reactive spray cases. However, it is obvious that the omission of the remap-PDF is also very helpful for emission prediction, such as soot, where the deviation from pre-known PDFs is often even more significant [24]. Note that the functional form of the scalar dissipation rate (f in Figure 3) is another important assumption, which could be also fully evaluated by means of PIESRGAN. However, a commonly used presumed log-based reference shape was used in this study.

FIGURE 3 Schematic representation of the MRIF approach. Tilde denotes Favre-filtered data. The overbar indicates Reynolds-averaging. The hat labels quantities in mixture fraction space. Z is the mixture fraction, W_i the flamelet weights, p the pressure, χ the scalar dissipation rate, ρ the density, Y_α the mass fractions, e the internal energy, and T the temperature. β denotes the presumed β-PDF, and f indicates the functional form of the scalar dissipation rate. The spatial coordinates are represented by $\vec{x}$, and integration over the volume of the full domain is described by $\int \mathrm{d}\vec{V}$. All variables are time dependent, but t is omitted here for brevity.

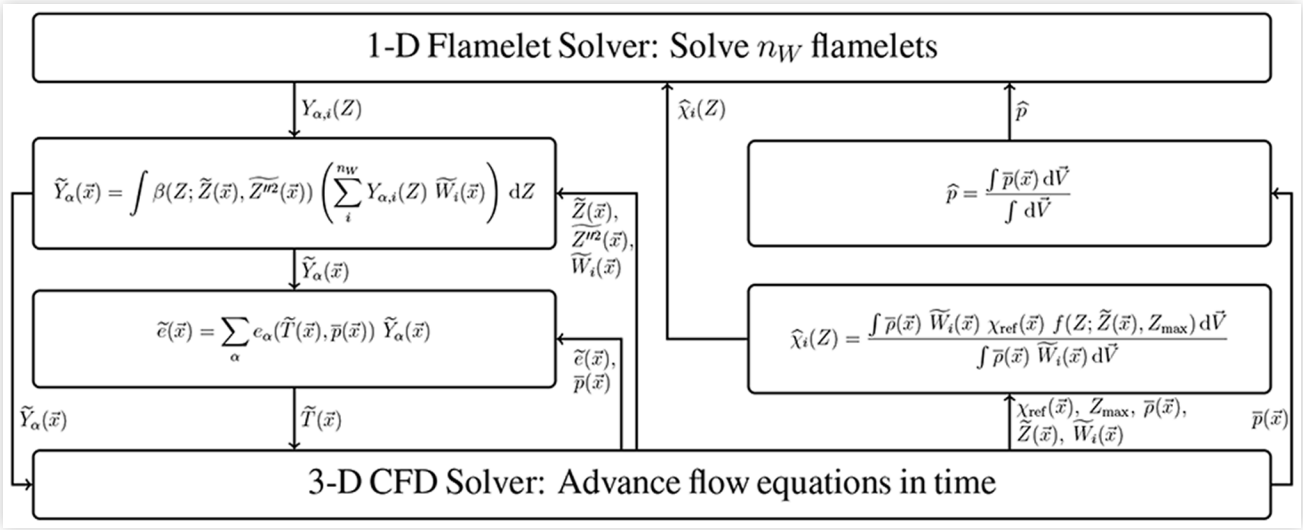

© Mathis Bode

Turbulence Data

For this work, the PIESRGAN was trained with one of the largest existing decaying turbulence DNS datasets [27] featuring velocity and scalar flow fields. The dataset consists of periodic boxes of homogeneous isotropic turbulence with Reynolds numbers based on the Taylor microscale Re_λ of up to 88, simulated on 4096^3 mesh points. Turbulent structures and their decay are illustrated for the used case in Figure 4.

FIGURE 4 Visualization of turbulent structures and their decay over time from an early time step (left) to a late time step (right). Obviously, while the number of structures decreases over time, their size increases. The relevant turbulence length scales - Kolmogorov length η and Taylor length l_t - also grow.

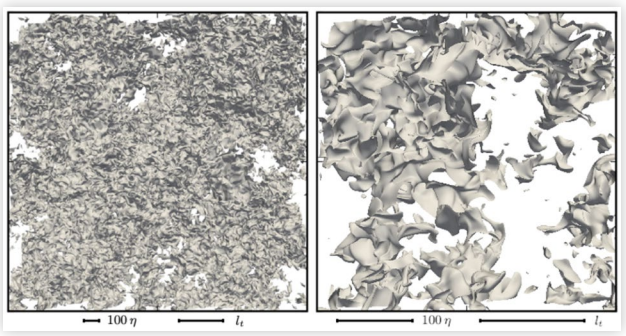

© Mathis Bode

Implementation Details

All application cases and testing were performed using the inhouse code CIAO. CIAO is astructured finite difference code with multiple solvers, such as a low-Mach solver and a compressible solver, which was used in this work. It utilizes staggering, and several multi-physics effects, such as chemistry and multiphase effects, can also be considered while solving the Navier-Stokes equations. Both DNS and LES can be performed with the same code framework, allowing for efficient development of LES models. Examples for successful multi-physics DNS [28, 29], multi-scale applications [30-32], and computing optimizations [33, 34] with CIAO can be found in the literature.

With respect to PIESRGAN, an implemented network can be found on GIT (https://git.rwth- aachen.de/Mathis.Bode/PIESRGAN.git) in order to increase the reproducibility of this work and clarify more technical details.

Discussion

This chapter discusses certain aspects of PIESRGAN. First, the universality and the generality are addressed. Afterwards, the accuracy of predicting mixing is investigated. Finally, the performance of PIESRGAN during training and on runtime is shown quantitatively.

Universality and Generality

The universality of data-based methods is always known to be a critical issue. This is true with respect to validity outside

the training data domain as well as with regards to various physical configurations, such as combustion type. In the field of turbulence modeling, this is particularly critical, since on the one hand, it is not possible to create data sets with arbitrarily high Reynolds number due to computational costs, and, on the other hand, many industrial applications have extremely high Reynolds numbers, for example, to increase the mixing rate.

Bode et al. [20] have presented a two-step training approach to increase the universality of PIESRGANs. In this approach, first, the generator network and the discriminator network are trained simultaneously with H/F data pairs. In the second step, the generator network is further optimized with S-data. In this case, S-data are under-resolved turbulence data at larger Reynolds numbers, for which no high-resolution reference data are available. Here, the generator loss function reduces to the physically motivated loss term and the adversarial loss term. If there is no physically motivated boundary condition for the target variable, as may be the case for passive scalars, even only the adversarial loss term remains, since the generator loss function and the significance of this term is clear. The basic idea is that this term ensures that certain features intrinsic to turbulence, which the discriminator network has learned from the high-precision data and passes on via the adversarial loss term, remain in the optimized generator network.

A similar generalization approach can be followed with respect to different physical configurations, again benefiting from the advantage of GANs over simpler DL networks: First, a PIESRGAN is trained with the basic H/F training data. Then, the physically motivated loss terms are updated, and S-data is used to optimize the generator network for the actual application. The S-data here can refer to data pairs, e.g., separate DNS data, or only simple training data. Again, the adversarial term is of great importance, since it acts as a corrective to ensure that certain turbulence features remain fulfilled in the final network. The procedure is also summarized in Table 2.

Mixing

The mixing process is especially critical for spray combustion cases. In the limit of the modeling approach discussed here, the following consecutive processes take place: the continuous liquid fuel phase split into smaller ligaments and successively into small droplets. In this disperse phase, the liquid fuel evaporates and starts mixing with the ambient gas phase. Ultimately, the combustion processes occur. The larger the resulting flame lift-off length (LOL) is relatively to the liquid penetration length (LPL), the more the resulting combustion is similar to classical non-premixed combustion, which is dominated by mixing processes. Thus, for spray combustion cases with sufficiently fast evaporation processes (one factor for a sufficiently large LOL and short LPL), accurate prediction of gas-phase mixing is one of the most important factors for predictive combustion simulations. As the evaluation of these mixing processes is very challenging under real engine spray conditions, especially, due to the lack of experimental data at these conditions, a simpler DNS case is used here for further discussion of PIERSGAN performance for predicting such processes.

TABLE 2 Summary of the PIESRGAN training strategy with respect to different update steps.

Step	Action	Data	Update
1	Base training	H/F	Generator & Discriminator
2	Special training	S	Generator

Figure 5 shows the mixture fraction PDF of a reactive, time-evolving methane jet mixing with air and simultaneously incinerating. The Reynolds number of the case is 10,000 and the Damköhler number is 0.15. Details of the DNS have been described by Denker et al. [29, 35]. For the a posteriori test, an early DNS solution, which was not used for training, was filtered and stored on a grid smaller by a factor of 64. This field was then temporally evolved using LESs with different subfilter models. Notably, the PIESRGAN-LES is able to correctly predict the mixing rate after the simulation was advanced for some time. The resulting PDF is very close to the PDF calculated on the DNS-data. In contrast, the classical LES without special LES mixing model significantly underestimates the mixing rate due to the underestimation of the local turbulence intensity. Overall, the PIESRGAN model gives a much better result, indicating that it should also significantly improve the prediction performance of spray-LES, if the combustion region is dominated by gas-phase mixing.

Training Performance

Computational costs are another critical issue worth discussing in the context of PIESRGANs. This concerns both the costs of training the GAN and of using it as a model during an LES. In the long run, the recurring costs as an LES model are more pivotal to the widespread use of a PIESRGAN-LES-model, although training costs are not negligible. In addition to the aforementioned costs, costs of creating the high-resolution data may also incur, if applicable. However, these will not be considered further here, as it is assumed that PIESRGANs will be used on existing data.

Figure 6 compares the training performances of PIESRGANs on different computing clusters. The computing cluster "JURECA" uses the Tesla K80 GPU, whereas the two

FIGURE 5 A posteriori test results for mixing prediction of a time-evolving methane jet for different LES subfilter scale models. "LES" corresponds to a "classical" LES with dynamic Smagorinski model.

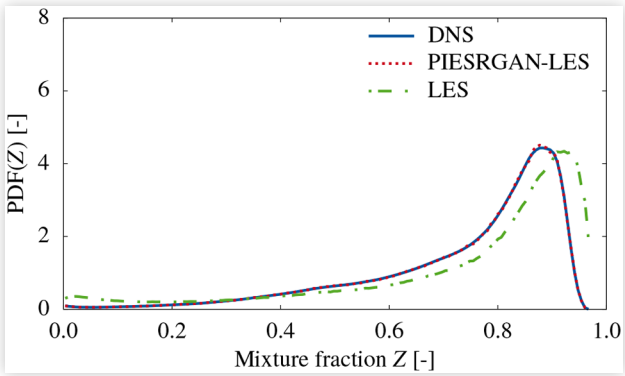

FIGURE 6 Comparison of the PIESRGAN training performance for different computing clusters and GPUs.

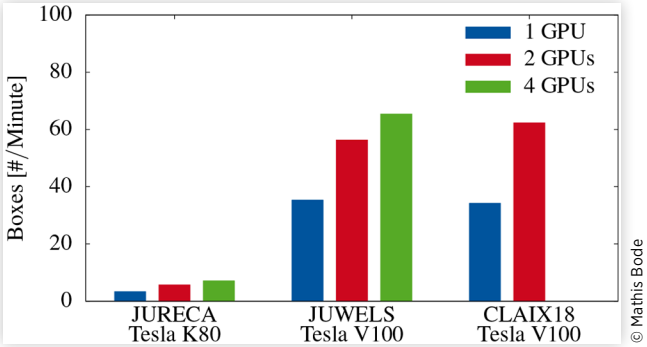

FIGURE 7 Comparison of PIESRGAN runtime costs for different target scenarios.

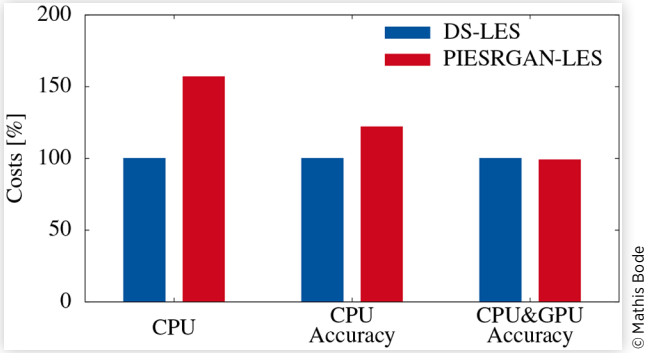

computing clusters "JUWELS" and "CLAIX18" use the newer Tesla V100 GPU. Up to four GPUs per compute node can be used for training (for CLAIX18, only a maximum of two GPUs is available). Boxes with a total of 4096 data points per data field were used as input during training, and the figure illustrates the number of boxes that can be processed per minute per compute node. The speed of newer GPU generation is striking for the PIESRGAN use case, which is also in line with the theoretical benchmark results and underlines the rapid development in this area. It is clear that due to this rapid development, the network training costs will continue to decrease relative to the costs of applying the model in an LES context, shifting the focus further towards runtime performance comparisons as discussed in the following sections.

Runtime Performance

The available computing capacities have been increased tremendously over the last years. At the Jülich Supercomputing Centre (JSC) [36], one of Germany's three big supercomputing facilities, the performance increased from 5.9 PFlop/s (JUQUEEN) to over 70 PFlop/s (JUWELS). However, from a fluid dynamic perspective, the development is not as distinct. Mostly due to bad cache usage because of complex stencils and the lack of sparse matrices for multi-physics cases, the actual performance of complex computational fluid dynamics (CFD) codes is often only 2%-5% of the theoretical LINPACK peak performance [33], even on clusters without GPUs. Unfortunately, for CFD applications, the major performance increase of almost all new clusters is by GPUs. For example, one JUWELS compute node features two AMD Epyc Rome CPUs but four Nvidia A100 GPUs. Thus, it is not possible to benefit from the tremendous gain in computing capacities if GPUs cannot be efficiently used.

Figure 7 shows the relative costs related to the Spray C LES use case, which is further discussed in the next chapter. LES with PIESRGAN as a subfilter model and LES with a traditional dynamic Smagorinsky (DS) model are compared. The cost of DS-LES using only CPUs is defined as 100%. It can be seen that the PIESRGAN subfilter model is significantly more expensive. This is not surprising, since more operations, especially the evaluation of the reconstructed data using filtering, need to be performed. Bode et al. [20], however, demonstrated that LES with PIESRGAN require fewer data points than LES with DS model to achieve comparable accuracy for the early mixing in the domain. For that, they compared DS-LES and PIESRGAN-LES results for an inert case with experimental data. Therefore, a "fairer" comparison of the performance and runtime cost could be based on a prescribed accuracy with a flexible number of grid points per simulation instead of a fixed number of grid points per simulation without any accuracy requirement. Hence, the computational cost for PIESRGAN-LES compared to an LES with a similar accuracy instead of the same number of data points is more beneficial for the PIESRGAN-LES. Additionally, it is important to consider that users often cannot choose the perfect computing cluster but are required to make use of what is available to them. Modern computing clusters usually have many GPUs, which are difficult to use with traditional LES models, leading to many unused FLOPS in the case of commonly employed CFD modeling. However, using them in the context of PIESRGAN is relatively straightforward. Thus, both approaches become similarly expensive under the conditions of equal accuracy and a combined CPU & GPU computing cluster available. It is particularly interesting that PIESRGAN modeling can also be seen as a change in the general computational approach, since cache-intensive operations, typical of ordinary flow solvers, are reduced and instead more computation time is required in tensor-heavy operations. Figure 6 illustrates the rapid development in tensor-heavy operations. Thus, as an outlook, it is not unlikely that this computational approach will benefit much more from future hardware improvements in terms of a shorter time to solution, even surpassing the conventional models.

Application

Simulations for multiple ambient temperatures were performed for the ECN Spray C case. The same mesh as in Bode et al. [20] was used, as well as the same mechanism by Yao et al. [37]. PIESRGAN dealt as LES-model for velocity and scalars, including, as mentioned, the remap subfilter-PDF. The nozzle internal flow has not been computed; however, the effective orifice diameter was reduced by the volume-based amount of

TABLE 3 Summary of different spray-LES simulation approaches.

Work	Davidovic et al. [22]	Goeb et al. [26]	Bode et al. [20]	Here
Initial droplets	Droplet distribution	Blob with nozzle diameter	Droplet distribution	Blob with effective liquid diameter (volume based)
Breakup	KH/RT	KH/RT	KH/RT	KH/RT
Evaporation	Bellan	Bellan	Bellan	Bellan
Velocity closure	Dynamic Smagorinsky	Dynamic Smagorinsky	PIESRGAN	PIESRGAN
Mixing closure	Dynamic Smagorinsky	Dynamic Smagorinsky	PIESRGAN	PIESRGAN
Combustion model	MRIF	MRIF	MRIF	MRIF
Subfilter PDF	Presumed beta-PDF	Presumed beta-PDF	Presumed beta-PDF	PIESRGAN
Dissipation form	Presumed log-based	Presumed log-based	Presumed log-based	Presumed log-based

known cavitation at the exit [23]. Breakup and evaporation models were the same as in the spray setup conducted by Goeb et al. [26]. The simulation setup is summarized in Table 3 in comparison to simulation setups employed in earlier work. Details regarding the used models can be found there. Note that even if the same breakup models were utilized in all simulations, their effect differs. Typically, a prescribed droplet distribution results in "very small" droplets very early in the domain, resulting in a small impact of the breakup models. In these cases, even the sensitivity with respect to the evaporation model is small, as the droplets quickly reach a lower cut-off diameter. For cases with blob injection, the breakup and evaporation models play a larger role.

Four different operation points with different ambient temperatures were considered in order to assess whether the PIESRGAN is as accurate as expected and whether the correct trends can be reproduced. The different cases are labeled by their ambient temperature in Kelvin as SC900, SC1000, SC1100, and SC1200. The other nominal conditions are identical among all cases with *n*-dodecane as fuel, 150 MPa injection pressure, 22.8 kg/m^3 ambient density, 15% ambient oxygen concentration, and 363 K fuel temperature. Note that in all simulations, actual measurement data were used instead of the nominal values to improve the comparability to experimental data.

Figure 8 compares the LOLs of the different cases over time. As expected, the LPL reduces with increasing temperature, as the evaporation process is accelerated. Interestingly, for long timings, the liquid penetration of SC1200 becomes larger than that of SC1100. However, the separation between these two cases is not large and only one realization has been run, limiting the statistical validity of the results.

Figures 9 and 10 compare the resulting LOL and ignition delay time with experimental data [23] for all four cases. The simulation is generally able to predict the trend correctly, which depicts that both LOL and ignition delay time reduce with increasing temperature. However, all values are slightly underpredicted. A similar result was found by Bode et al. [20], which might be attributed to the used chemical mechanism that strongly affects both quantities. Finally, Figures 8-10 allow the

FIGURE 8 Comparison of the resulting LPL from simulations with different ambient temperatures for the considered Spray C case.

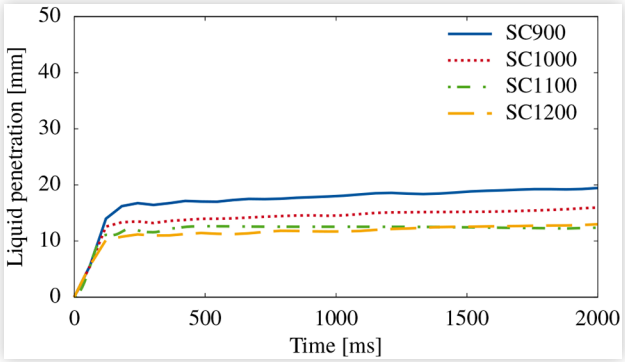

FIGURE 9 Comparison of the resulting LOL from simulations and experiments for the considered Spray C cases.

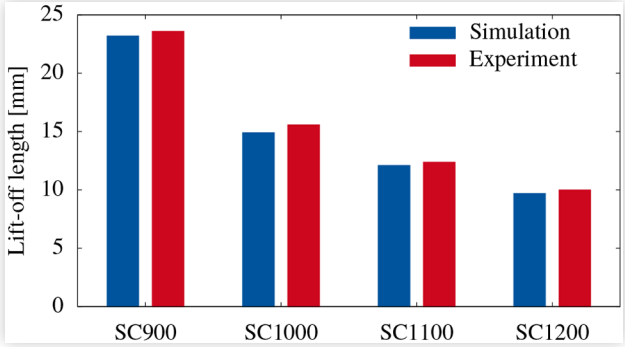

FIGURE 10 Comparison of the resulting ignition delay time from simulations and experiments for the considered Spray C cases.

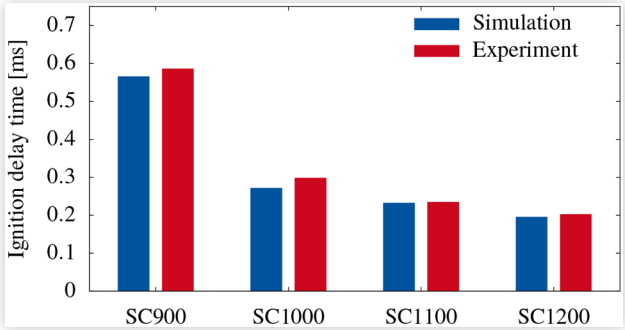

conclusion that for the ECN Spray C case, the relative separation of LOL and LPL seems sufficient for the standard single-phase mixing approach, as discussed earlier.

Summary/Conclusions

This paper demonstrates the application of PIESRGAN to the ECN Spray C case. The presented simulations are able to capture experimental data reasonably and could be used as basis for further physical analyses of the ECN Spray C case. The discussion focus of this work was on the computational and numerical aspects of PIESRGAN-LES. The accuracy of PIESRGAN-based mixture prediction is fair; however, its implementation requires more computing operations per execution. In this context, the computational performance on current GPU-heavy supercomputers was addressed.

References

1. Kutz, J., "Deep Learning in Fluid Dynamics," *Journal of Fluid Mechanics* 814 (2017): 1-4.
2. Hinton, G., Deng, L., Yu, D., Dahl, G. et al., "Deep Neural Networks for Acoustic Modeling in Speech Recognition," *IEEE Signal Processing Magazine* 29 (2012).
3. Wang, X., Yu, K., Wu, S., Gu, J. et al., "ESRGAN: Enhanced Super-Resolution Generative Adversarial Networks," *Lecture Notes in Computer Science* 11133 (2019): 63-79.
4. Vinyals, O., Babuschkin, I., Czarnecki, W., Mathieu, M. et al., "Grandmaster Level in StarCraft II Using Multi-Agent Reinforcement Learning," *Nature* 575 (2019): 350-354.
5. Dong, C., Loy, C.C., He, K., and Tang, X., "Learning a Deep Convolutional Network for Image Super-Resolution," in *European Conference on Computer Vision*, pp. 184-199, Springer, 2014.
6. Bhati, A., Wan, S., Alfe, D., Clyde, A. et al., "Pandemic Drugs at Pandemic Speed: Infrastructure for Accelerating COVID-19 Drug Discovery with Hybrid Machine Learning- and Physics-Based Simulations on High Performance Computers," *Interface Focus* (2021): 20210018.
7. Parish, E.J. and Duraisamy, K., "A Paradigm for Data-Driven Predictive Modeling Using Field Inversion and Machine Learning," *Journal of Computational Physics* 305 (2016): 758-774.
8. Srinivasan, P., Guastoni, L., Azizpour, H., Schlatter, P. et al., "Predictions of Turbulent Shear Flows Using Deep Neural Networks," *Physical Review Fluids* 4, no. 5 (2019): 054603.
9. Maulik, R. and San, O., "A Neural Network Approach for the Blind Deconvolution of Turbulent Flows," *Journal of Fluid Mechanics* 831 (2017): 151-181.
10. Bode, M., Gauding, M., Göbbert, J., Liao, B. et al., "Towards Prediction of Turbulent Flows at High Reynolds Numbers Using High Performance Computing Data and Deep Learning," *Lecture Notes in Computer Science* 11203 (2018): 614-623.
11. Lapeyre, C.J., Misdariis, A., Cazard, N., Veynante, D. et al., "Training Convolutional Neural Networks to Estimate Turbulent Sub-Grid Scale Reaction Rates," *Combustion and Flame* 203 (2019): 255-264.
12. Bode, M., Gauding, M., Kleinheinz, K., and Pitsch, H., "Deep Learning at Scale for Subgrid Modeling in Turbulent Flows: Regression and Reconstruction," *LNCS* 11887 (2019): 541-560.
13. Bode, M., et al., "Development of Physics-Informed Enhanced Super-Resolution Generative Adversarial Networks for Subfilter Modeling," *arXiv preprint*, 2021.
14. Raissi, M., Perdikaris, P., and Karniadakis, G., "Physics-Informed Neural Networks: A Deep Learning Framework for Solving Forward and Inverse Problems Involving Nonlinear Partial Differential Equations," *Journal of Computational Physics* 378 (2019): 686-707.
15. Banerjee, I. and Ierapetritou, M.G., "An Adaptive Reduction Scheme to Model Reactive Flow," *Combustion and Flame* 144, no. 3 (2006): 619-633.
16. Ihme, M., Schmitt, C., and Pitsch, H., "Optimal Artificial Neural Net- Works and Tabulation Methods for Chemistry Representation in LES of a Bluff-Body Swirl-Stabilized Flame," *Proceedings of the Combustion Institute* 32 (2009): 1527-1535.
17. Bode, M., Collier, N., Bisetti, F., and Pitsch, H., "Adaptive Chemistry Lookup Tables for Combustion Simulations Using Optimal b-Spline Interpolants," *Combustion Theory and Modelling* 23, no. 4 (2019): 674-699.
18. Seltz, A., Domingo, P., Vervisch, L., and Nikolaou, Z.M., "Direct Mapping from LES Resolved Scales to Filtered-Flame Generated Manifolds Using Conv. Neural Networks," *Combustion and Flame* 210, no. 12 (2019): 71-82.
19. Wang, Q. and Ihme, M., "A Regularized Deconvolution Method for Turbulent Closure Modeling in Implicitly Filtered Large-Eddy Simulation," *Combustion and Flame* 204, no. 6 (2019): 341-355.
20. Bode, M., Gauding, M., Lian, Z., Denker, D. et al., "Using Physics-Informed Enhanced Super-Resolution Generative Adversarial Networks for Subfilter Modeling in Turbulent Reactive Flows," *Proceedings of the Combustion Institute* 38 (2021): 2617-2625.
21. Goodfellow, I., Pouget-Agadie, J., Mirza, M., Xu, B., et al., "Generative Adversarial Networks," *arXiv:1406.2661*, 2014.
22. Davidovic, M., Falkenstein, T., Bode, M., Cai, L. et al., "LES of n-Dodecane Spray Combustion Using a Multiple Representative Interactive Flamelets Model," *Oil Gas Science and Technology* 72, no. 29 (2017).
23. "Engine Combustion Network," 7, Workshop https://ecn.sandia.gov/ecn-workshop/ecn7-workshop, accessed on 2021-09-04.
24. Kolmogorov, A.N., "Dissipation of Energy in Locally Isotropic Turbulence," *Dokl. Akad. Nauk SSSR* 32 (1941): 16-18.
25. Kolmogorov, A.N., "The Local Structure of Turbulence in Incompressible Viscous Fluid for Very Large Reynolds Numbers," *Dokl. Akad. Nauk SSSR* 30 (1941): 299-303.
26. Goeb, D., Davidovic, M., Cai, L., Pancharia, P. et al., "Oxymethylene Ether - n-Dodecane Blend Spray Combustion: Experimental Study and Large-Eddy Simulations," *Proceedings of the Combustion Institute* 38 (2021): 3417-3425.

27. Gauding, M., Wang, L., Goebbert, J.H., Bode, M. et al., "On the Self-Similarity of Line Segments in Decaying Homogeneous Isotropic Turbulence," *Computers & Fluids* 180 (2019): 206-217.
28. Falkenstein, T., Kang, S., Cai, L., Bode, M. et al., "DNS Study of the Global Heat Release Rate During Early Flame Kernel Development Under Engine Conditions," *Combustion and Flame* 213 (2020): 455-466.
29. Denker, D., Attili, A., Boschung, J., Hennig, F. et al., "Dissipation Element Analysis of Non-Premixed Jet Flames," *Journal of Fluid Mechanics* 904 (2020): A4.
30. Bode, M., Diewald, F., Broll, D., Heyse, J. et al., "Influence of the Injector Geometry on Primary Breakup in Diesel Injector Systems," SAE Technical Paper 2014-01-1427 (2014). https://doi.org/10.4271/2014-01-1427.
31. Bode, M., Falkenstein, T., Le Chenadec, V., Kang, S. et al., "A New Euler/Lagrange Approach for Multiphase Simulations of a Multi-Hole GDI Injector," SAE Technical Paper 2015-01-0949 (2015). https://doi.org/10.4271/2015-01-0949.
32. Bode, M., Falkenstein, T., Davidovic, M. et al., "Effects of Cavitation and Hydraulic Flip in 3-Hole GDI Injectors," *SAE International Journal of Fuels and Lubricants* 10, no. 2 (2017): 380-393.
33. Bode, M., Davidovic, M., and Pitsch, H., "Multi-Scale Coupling for Predictive Injector Simulations," in: , *High-Performance Scientific Computing*, (Springer Int. Publishing, 2017), 96-108.
34. Bode, M., Davidovic, M., and Pitsch, H., "Towards Clean Propulsion with Synthetic Fuels: Computational Aspects and Analysis," in: , *High-Performance Scientific Computing*, (Springer Nature, 2019), 185-207.
35. Denker, D., Attili, A., Gauding, M., Niemietz, K. et al., "A New Modeling Approach for Mixture Fraction Statistics Based on Dissipation Elements," *Proceedings of the Combustion Institute* 38 (2021): 2681-2689.
36. "Jülich Supercomputing Centre," https://www.fz-juelich.de/ias/jsc/EN/Home/homenode.html, accessed 2021-09-04.
37. Yao, T., Pei, Y., Zhong, B.-J., Som, S. et al., "A Compact Skeletal Mechanism for n-Dodecane with Optimized Semi-Global Low-Temperature Chemistry for Diesel Engine Simulations," *Fuel* 191 (2017): 339-349.

Contact Information

Mathis Bode
Jülich Supercomputing Centre
Forschungszentrum Jülich GmbH
RWTH Aachen University
m.bode@itv.rwth-aachen.de

Acknowledgments

The author kindly acknowledges the computing time awarded as part of the JARA-HPC partition on JURECA/JUWELS/CLAIX18 under grants "TurbulenceSL" and "jhpc55" at Jülich Supercomputing Centre, Forschungszentrum Jülich, and RWTH Aachen University. Furthermore, funding from the European Union's Horizon 2020 research and innovation program under the Center of Excellence in Combustion (CoEC) project, grant agreement no. 952181 is acknowledged.

e-ISSN 2641-9645